Combustion and Flame 229 (2021) 111374

Contents lists available at ScienceDirect

Combustion and Flame

journal homepage: www.elsevier.com/locate/combustflame

Modelling reaction propagation for Al/CuO nanothermite pellet combustion

Joseph Mark Epps[a], Jean-Pierre Hickey[a,*], John Z. Wen[a]

Department of Mechanical and Mechatronics Engineering, University of Waterloo, 200 University Avenue West, Waterloo N2L3G1, Canada

ARTICLE INFO

Article history:
Received 9 October 2020
Revised 16 February 2021
Accepted 17 February 2021

Keywords:
Al/CuO
Nanothermite
Propagation
Porosity
Numerical simulation

ABSTRACT

A continuum-scale model for the combustion of consolidated nanothermite pellets is introduced. A simplified chemical kinetics model is used for the solid state nanothermite reaction while a two-phase porous media flow accounts for the mass and heat transfer within the consolidated pellet under an equilibrium thermodynamic assumption. The thermophysical and chemical kinetic properties of the Al/CuO nanothermite pellets are determined from the literature. A sensitivity analysis reveals the relative importance of these modelling parameters for both the advection and conduction-dominated combustion regimes. Based on the governing equations, we propose a thermodynamically consistent non-dimensionalization of the global Peclet and Damköhler numbers which are based on the characteristic Darcy velocity within the porous pellet. The non-dimensionalization results in a linear scaling between the normalized burn rate and Peclet number, which allows a collapse of the numerical results with published experimental data. We identify a transition between the conduction- and advection-dominated combustion based on the transient burn rate of the nanothermite pellet combustion.

1. Introduction

Nanothermite mixtures are made up of nano-sized metallic fuel and inorganic oxidizer components. As this solid mixture represents a metastable intermolecular composite, an increase in nanothermite temperature can initiate a chemical reorganization which is highly exothermic and results in the formation of a stable oxide and a free metal. As the oxidation usually starts on the surface of nanoparticles, the nanothermite composite is characterized by a very high reactivity compared to other type of solid propellants such as their micro-sized counterparts. Furthermore, as their geometries and chemical compositions are highly tuneable, so are their burning characteristics. These properties are well suited for a number of engineering applications such as pyrotechnics, igniters, explosives, and propellants.

Nanothermites are commonly fabricated by physically mixing the commercially available metal and metal-oxide powders, which is subsequently pressed into fuel pellets. Ignition occurs when the pellets are heated (usually with a laser or a hot wire), which initiates a self-sustaining exothermic reaction through the pellet. The reaction front propagation in a burning nanothermite pellet ranges from 1 to 1000 ms^{-1} and the burn rate has been shown to be highly dependent on the pellet packing density [1–3]; though, the exact mechanism(s) responsible for the dramatic variation in burn rates remains subject to debate [4]. The literature generally accepts two dominant burning regimes where the reaction propagation is defined, to varying degrees, as either convection or conduction dominating [4,5]. Being consolidated metallic pellets, conduction of heat is a natural means to advance the reaction front by raising the temperature of the unburnt nanothermite pellet to ignition temperature; the timescale of conductive heat transfer is governed by the thermophysical properties of the pellet. Pores, due to the imperfect contact of the compressed nanoparticles within the pellets, reduce the thermal conductivity and hence inhibit heat conduction. The second mean of reaction front propagation is pressure-driven advection of high temperature combustion products (convection) through the porous pellet. Note that the advection affects both heat and mass transfer. Although increased porosity can enhance the advection-driven reaction front propagation, it also results in a lower energetic density of the nanothermite pellet. Sanders et al. [1] observed decreasing burn rates with increasing packing density in Al/MoO3 nanothermite specimens, suggesting impeded advection at higher densities. Saceleanu et al. [3] also observed a similar trend with Al/CuO pellets. Advection in a porous medium highly depends on the local pressure gradient. Weismiller et al. [4] observed decreasing burning rates with increasing ambient pressures in Al/CuO; as the pressure gradient drives the mass flow through the porous medium, increasing the ambient pressure

* Corresponding author.
E-mail address: jean-pierre.hickey@uwaterloo.ca (J.-P. Hickey).

https://doi.org/10.1016/j.combustflame.2021.02.020
0010-2180/

should naturally inhibit advection. Further scaling analysis done by Weismiller et al. [4] with Fourier, Darcy and the ideal gas laws confirmed that in addition to conduction, advection or convection is also a primary propagation mode. Therefore it is clear that, from the perspective of heat transfer, a combination of conduction and convection mechanisms help sustain the reaction front propagation within a reacting nanothermite pellet.

Convective heat transfer (via advecting fluids) associated with nanothermite combustion is important but also necessitates a large pressure gradient to drive the flow. The advection within a porous pellet is mainly driven by the pressure rise associated with the gas formation of the thermite reaction. This has been calculated by Fischer and Grubelich [6] where significant amounts of gas are generated from certain thermite reactions. A number of experiments [1,2,4,7] reported on the pressure generation when aluminum reacted with copper, molybdenum, bismuth and tungsten oxides. Reaction equilibrium models developed by Baijot et al. [8] also addressed gas generation from thermite reactions. Although Egan and Zachariah [5] suggested the convective heat transfer by gases is not sufficient to sustain the high burn rates in less dense pellets, there is still a need to consider the roles of both conduction and advection in reaction propagation of a burning nanothermite pellet.

Efforts in modelling nanothermite combustion have been undertaken despite an incomplete understanding of the tightly-coupled physical phenomena arising in this problem. Umbrajkar et al. [9], Ermoline and Schoenitz [10], and Stamatis et al. [11] attempted to model low-temperature ignition of nanothermite specimens using CuO decomposition and alumina phase transformation. The kinetic parameters were adjusted using their respective Differential Scanning Calorimetry (DSC) results which found that the rate determining steps during the reaction changed at different temperatures corresponding to different mechanisms. A detailed mechanism for the same thermite was developed by Baijot et al. [12] involving phase changes, ambient oxygen effects, CuO decomposition and the impact of alumina. These studies focused on the reaction kinetics and material phase change and not on the reactive front propagation within a compressed, nanothermite pellet. Other works have taken an engineering approach to better understand the aggregate effects of nanothermite powder or pellet combustion. In this context, the intrinsic chemical mechanisms are often simplified and become of secondary importance compared to the coupled multi-physics interactions affecting the reactive front propagation. To augment their experimental findings, Nicollet et al. [13] and Stacy et al. [14] used the heat equation to contrast the expected thermal behaviour to their findings. Kim [15] used an one-dimensional continuum heat transfer model to characterize nano- and micro-scale Al/MoO3 thermites. The reaction details were simplified into a single source term in the heat equation with a reaction progress variable. Knapp et al. [16] recently used their developed Hot Spot model to capture propagation rates based on equivalence ratio and particle sizes. Although these researchers have taken a meta-scale approach to model the nanothermite combustion, the effect of porosity, which introduces a mode of convective heat transfer within the pellet, has not been addressed.

This paper introduces a continuum model to study the phenomena governing laser-ignited porous Al/CuO nanothermite pellets. This numerical study is done in support of our previous experimental investigations on Al/CuO nanothermites [3]. The numerical framework incorporates the important physical processes including porous media transport in the self-sustaining combustion of the pellets. Many of the proposed thermophysical or chemical kinetic models are derived from previously published experimental works. The objective herein is to enable a parametric investigation of the important physical characteristics of nanothermite pellet combustion which subsequently help develop engineering applications for new nanothermite composites. To this end, the next section will discuss the governing equations and modelling assumptions as well as present a consistent non-dimensionalization. Section 3 will focus on the implementation of these physical models into the numerical framework; the validation of the framework is addressed in Section 4. The primary results and discussion are in Section 5 and the concluding remarks are left for Section 6.

2. Modelling and non-dimensional analysis

A framework is developed to model, at a continuum scale, the ignition and subsequent reaction propagation in a consolidated Al/CuO nanothermite pellet. The governing equations along with the corresponding thermophysical models and source term are combined within this numerical framework. The solver, although developed for Al/CuO thermite pellet combustion, is generalizable to any gas-generating nanothermite reaction modelled at a continuum scale. In this section, we first present the governing equations and thermophysical models implemented in this framework. Then, based on these models, the dimensionless parameters driving the combustion processes are proposed.

2.1. Governing equations and modelling assumptions

2.1.1. Mass and momentum conservation

Nanothermite pellets are porous due to the aggregation and imperfect compression of the nanothermite powders. The chemical reactions generate liquid, solid and gas phase products at the combustion temperature, while some residual reactants remain in a solid phase. The liquid product can solidify upon cooling. To simplify this process, a two-phase, continuum model was adopted to focus on the gas and non-gas phases; termed *gas* and *solid (or condensed)* phases respectively. The equivalent reaction equation of the process is:

$$\mathrm{A_{(s)}} \rightarrow \mathrm{B_{(s,l)}} + \mathrm{C_{(g)}} \tag{1}$$

where A is the *solid* phase reactants, B is the *solid/condensed* phase products and C is the *gas* phase product. At the expected temperatures of nanothermite combustion, formation of the liquid and gaseous products can change the original porosity of the pellet. However for these rapidly occurring thermite reactions, it is reasonable to assume the volume change caused by liquid formation can be compensated by the reduced space occupied by the solid reactants, which leaves the same pore volume to the gaseous product. Most gases have the similar thermal behaviour, so the initial ambient gas already present within the porous material is lumped into the *gas* phase with the produced gases from combustion (C in Eq. (1)). The mass conservation equation for the phases, denoted with the subscripts s (solid) and g (gas), are:

$$\frac{\partial \rho_s}{\partial t} = -\dot{\rho}_{g,source} \tag{2a}$$

$$\frac{\partial \rho_g}{\partial t} + \nabla \cdot (\rho_g \mathbf{u}) = \dot{\rho}_{g,source} \tag{2b}$$

where $\mathbf{u}$ is the vector of the fluid velocity, and $\dot{\rho}_{g,source}$ is the source term representing the gas production. For this model, all products are generated from the solid reactants, hence the source terms in both the gas and solid phases have equal magnitudes but opposite signs.

As the advection of gas within the porous pellet is driven by the pressure gradient resulting from the nanothermite reaction, we rely on Darcy's law to compute the advection velocity through the porous medium of the pellet:

$$\mathbf{u} = -\frac{K}{\mu}\nabla P \tag{3}$$

where P is the pressure, K is the permeability of the solid, and μ is the viscosity of the gas. The pore Reynolds number being small at the scales under consideration, we neglect any inertial effects in the pressure-driven porous flow.

The permeability in Eq. (3) is usually experimentally determined for porous media. As we have very limited experimental permeability results for nanothermites pellets, the Kozeny-Carmen equation [17] allows us to relate the porosity of a packed bed of uniform spheres to its permeability for porous structures. The Kozeny-Carmen equation is given by:

$$K = \frac{\phi^3 d_c^2}{k_k(1-\phi)^2} \tag{4}$$

where ϕ is the porosity, d_c is the ratio between solid volume and fluid-solid interfacial surface area (will be referred to as characteristic pore size) and k_k is the Kozeny constant. This relationship is a standard model for a packed bed of spheres however, in the present model, it permits an order of magnitude estimation of the permeability and resulting advection velocities given the porosity and characteristic pore sizes.

The pressure gradient driving the advective flow in Eq. (3) is the result of the formation and dilatation of the gas due to the reaction. As the gas pressure (more precisely its gradient) is driving the advective flow, we assume an ideal gas law relating the pressure, density, and temperature :

$$P = \frac{\rho_g RT}{\phi} \tag{5}$$

where R is the specific gas constant for the given gaseous composition. Since the variable density is given per volume of continuum, porosity must be included to reflect the pressure inside the pore. The *gas* and *solid* are assumed to be in thermal equilibrium and thus have equal temperatures. Thermal non-equilibrium effects could be considered in future works through the use of a segregated energy equation for gas and solid phases.

2.1.2. Energy conservation

The conservation of mass and momentum equations are supplemented by the conservation of energy. We assume the kinetic energy of the advecting fluid within the porous media to be negligible compared to the changes in internal energy of the system. Thus the conservation of energy is given by:

$$\frac{\partial \rho C_{eff} T}{\partial t} + \nabla \cdot (\rho_g \mathbf{u} C_{p,g} T) = \nabla \cdot \left(\lambda_{eff} \nabla T\right) + \dot{Q}_{source} \tag{6}$$

where $\rho C_{eff} = \rho_s C_{v,s} + \rho_g C_{v,g}$ is the energy storage contribution of the *solid* and *gas* phases, $C_{v,(g,s)}$ is the specific heat at constant volume for each phase, λ_{eff} is the effective thermal conductivity, $C_{p,g}$ is the specific heat at constant pressure for the *gas*, and $\dot{Q}_{source}$ is the heat generated due to the reaction, details of which are explained in the following section.

2.1.3. Source terms and thermophysical models

The heat generated from the reaction follows an Arrhenius form, as in Kim [15]:

$$\dot{Q}_{source} = \rho_{s,0} \dot{\eta} \Delta H \tag{7}$$

$$\dot{\eta} = A_0 (1-\eta) \exp\left(-\frac{E_a}{R_u T}\right) \tag{8}$$

where $\rho_{s,0}$ is the initial density of *solid*, ΔH is the enthalpy of combustion, A_0 is the pre-exponential factor, η is the reaction progress variable, Ea is the activation energy, and R_u is the universal gas constant. The initial density of the *solid* phase is calculated based on porosity and the Theoretical Maximum Density (TMD) by:

$$\rho_{s,0} = (1-\phi)\rho_{TMD} \tag{9}$$

There is some uncertainty for the values of the pre-exponential and activation energy in Eq. (8) due to the debate around the exact mechanism(s) of nanothermite combustion. This one-step Arrhenius equation is commonly accepted for modelling chemical reactions and is simple enough for implementation in this model. The exponential form of the Arrhenius equation provides a realistic functional form of the chemical kinetics, however the implications of using such a simplified, one-step model will be addressed in the discussion. The enthalpy of combustion is documented for stoichiometric thermite mixtures in Fischer and Grubelich [6]. In calculating these values, the reactions begin at 293 k and the final products are in liquid, gas or solid states. For the reactions with liquid products, the enthalpy of combustion includes the enthalpies of fusion of the products. Using the full enthalpy of combustion will overestimate the temperature since the melting of these products are not accounted for in the present model. Therefore, the enthalpy of combustion used should subtract the enthalpies of fusion of the liquid products to more accurately reflect the expected temperature.

Gas is known to be generated by nanothermite reactions based on experiments [1,2] and theory [6,8]. Furthermore, experiments often measure significant pressure increases which supports the idea of gas generation. The origins of the gas remain subject to debate as both oxygen from the oxidizer decomposition [18] or metal vapours [8] have been shown to contribute to the gaseous phase. From Eq. (8), the source terms for Eqs. (2a) and (2b) can be derived. The evolution of the global reaction is uniquely characterized by the progress variable, η, given the single-step reaction mechanism. We relate the rate of change of the progress variable to the gaseous source term production as:

$$\dot{\rho}_{g,source} = \dot{\eta} \rho_{g,f} \tag{10}$$

where $\rho_{g,f}$ is the known density of *gas* in the post-reaction state and $\dot{\rho}_{g,source}$ rate of gas generation. Given this formulation, we can understand the progress variable as an analogue of the density ratio in the system:

$$\eta = \frac{\rho_g - \rho_{g,0}}{\rho_{g,f}} \tag{11}$$

where $\rho_{g,0}$ is the initial density of *gas* present in the pores of the pre-combustion state. We note that in our solver, the evolution of the progress variable is not computed based on the density ratios but computed from the temporal integration of the Arrhenius equation.

To maintain thermodynamic consistency of the *solid* phase, the specific heat represents a weighted average (based on the reaction progresses variable) of the solid reactants and liquid products:

$$C_{v,s} = C_{v,s0}(1-\eta) + C_{v,s1}(\eta) \tag{12}$$

where $C_{v,s0}$ is a mass fraction weighted specific heat of the reactants at 293 K and $C_{v,s1}$ is a mass fraction weighted specific heat of the products at the adiabatic flame temperature. If the products are in the solid and/or liquid state at the adiabatic flame temperature (B phase in Eq. (1)), the specific heat is reflected in the value of $C_{v,s1}$. Specific heat capacity of solids and liquids are approximately constant with respect to temperature, so choosing fixed bounds is a reasonable approximation. For the *gas* phase, the exact composition is not known, so the specific heat of the *gas* was selected based on the expected composition of the gas.

The porous nature and changing composition of the pellet will have an impact on the effective thermal conductivity. In our numerical model, the effective thermal conductivity was assumed constant and determined based on possible theoretical values. More generally, the effective thermal conductivity can be estimated for a homogeneous two-phase mixture using the volume fraction contribution of each component. There exists many theories about

the effect of dispersed phases on effective properties for specific microstructure arrangements [19,20], however each method is associated with specific geometric considerations of the pores in the solid matrix. Since the structure of nanothermites is not easily quantified, choosing an appropriate model for thermal conductivity would prove difficult. As a result, our parametric investigation in the subsequent sections spans the bounds of realistic effective conductivity of a consolidated pellet.

2.2. Non-dimensional analysis

Based on the set of partial differential equations governing the physics of nanothermite pellet combustion, we provide a non-dimensionalization of the problem that is both kinetically and thermodynamically consistent. The proposed non-dimensionalization will help characterize the relative contributions of the heat transfer modes and time scales on the overall combustion.

For the nanothermite pellet combustion, we define the adiabatic temperature of reaction, T_{ad}, the ambient pressure, p_∞, and the specific heat of the *gas*, C_p as the characteristic thermodynamic variables governing this problem. These thermodynamic variables characterize the advective gas as well as the temperature driving the conductive heat transfer in the pellet. Note that the adiabatic flame temperature can be theoretically evaluated based on the thermophysical characteristics of the nanothermite; in the present Al/CuO nanothermite combustion, T_{ad} is set to 2844 K. Through the use of the ideal gas Eq. (5), we can define a characteristic density based on the preceding thermodynamic variables such that:

$$[T_{ref}] = T_{ad}, \quad [R_{ref}] = \frac{\gamma - 1}{\gamma}[C_{p,ref}], \quad [p_{ref}] = p_\infty,$$
$$[\rho_{ref}] = \frac{[p_{ref}]}{[R_{ref}][T_{ref}]} \tag{13}$$

Additionally, we define the characteristic length scale, $[L_{ref}]$ of the problem to be the height of the pellet, H. Although we acknowledge that other characteristic length scales could be used (e.g. pellet radius or pore size), we select the pellet height as it represents an easily quantifiable metric. Additionally, the characteristic length based on the height of the pellet can be used, in conjunction with the characteristic velocity, to estimate the total pellet burn time. The characteristic velocity is tied to the advective velocity of the fluid within the porous nanothermite pellet. The characteristic velocity is directly computed from the Darcy Eq. (3) which yields:

$$[U_{ref}] = \frac{K}{\mu}\frac{[p_{ref}]}{[L_{ref}]} \tag{14}$$

where the $\frac{K}{\mu}$ represents the ratio of the permeability, K, over the dynamic viscosity of the gas. The characteristic time scale of the problem is the ratio of the characteristic length to velocity scale: $[t_{ref}] = \frac{[L_{ref}]}{[U_{ref}]}$. The use of the ambient pressure to determine the characteristic velocity is slightly inconsistent with the experimental results [4] that showed a decrease in reaction front propagation with increasing ambient pressure. Future works may want to consider determining a characteristic pressure gradient or pressure difference in the porous media flow instead of relying uniquely on the ambient pressure.

By non-dimensionalizing the set of governing equations, and more particularly the energy conservation (Eq. (6)), the characteristic Peclet and Damköhler numbers emerge. These dimensionless numbers are used to respectively define the ratio of advective to conductive heat transfer and advective to chemical timescales of the problem. Based on the selected characteristic kinematic and thermodynamic quantities, we define:

$$Pe = \frac{[\rho_{ref}][U_{ref}][C_{p,ref}][L_{ref}]}{\lambda_{eff}} \tag{15}$$

$$Da = \frac{[L_{ref}]}{\tau_{chem}[U_{ref}]} = \frac{\mu}{K}\frac{[L_{ref}]^2}{\tau_{chem}[p_{ref}]} \tag{16}$$

Here, we define the τ_{chem} as the inverse of the exponential factor in the Arrhenius equation, $1/A_0$.

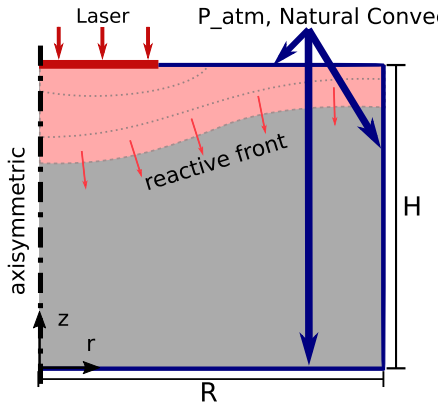

Fig. 1. Boundary conditions, characteristic dimensions of the simulation with illustration of the propagation of the reactive front (not to scale).

3. Simulation details and numerical framework

3.1. Simulation details

A two-dimensional, axisymmetric cylinder with a radius of 1 mm, and height of 6 mm was simulated to compare with experiments conducted at the University of Waterloo [3]. Compared to the experiments, the domain is larger in the axial direction in order to obtain a stable reaction propagation velocity in the pellet while minimizing the impact of the boundary condition on the simulation. Each simulation was run until at least 80% of the initial pellet had reacted; this ensures a proper averaged flame front velocity. A variable time advancement was selected to maintain computational stability; the variable time step size was selected to satisfy both the Fourier and Courant-Friedrichs-Lewy (CFL) conditions. Based on these stability constraints, the time-step of the simulation ranged between 1×10^{-10} and 1×10^{-8} s. The baseline computational domain was discretized using 1340 and 224 nodes in the axial and radial direction, respectively. This grid size provided an adequate balance between computational efficiency and required resolution. Spatial and temporal convergence studies were conducted and are presented in Section 4.

3.2. Boundary and initial conditions

The computational domain of the nanothermite pellet is shown in Fig. 1 along with the boundary conditions and an illustration of the reaction front propagation. Being an axisymmetric domain, a zero flux boundary condition is enforced along the centreline of the pellet. A constant heat flux, to represent the laser heating, is applied over a radius of 0.2 mm of the top boundary at middle of the pellet, the power of the laser ($400\,\mathrm{MWm^{-2}}$) is taken from Saceleanu et al. [3]. The constant heat flux is applied until a self-sustained ignition of the nanothermite is achieved at which point the heat flux is removed.

The remaining boundary conditions (blue boundaries in Fig. 1) on the pellet impose a Dirichlet boundary condition on the pressure. As a result a pressure gradient may develop at the boundary,

Table 1
Modelling parameters used in numerical study. Cited sources are provided when available.

Parameter	Baseline Case	Parametric study
$C_{v,g}, C_{p,g}, R$	$O_{2(g)}(T)$ [9,18]	$Cu_{(g)}$(2844 K), $Al_{(g)}$(2844 K) [8]
$dc \times 10^9$ [m]	40	100, 1000
$\mu \times 10^5$ [kg m^{-1} s^{-1}]	1	10, 100
$A_0 \times 10^{-6}$ [s^{-1}]	4.89 [9]	0.489, 2.44
E_a [kJ mol^{-1}]	48 [15]	70 [15], 80
λ_{eff} [Wm^{-1} K^{-1}]	65	1 [21], 100

which permits a gaseous mass flux leaving the computational domain; this boundary condition is selected to model the advective mass loss from the pellet to the atmosphere through the porous boundary walls. The thermal boundary conditions allow for natural convection on the pellet walls. The order of magnitude for natural convection of gases is around 1 to 10 Wm^{-2} K^{-1}. Even with this value over an expected temperature range of 2500 K, the heat loss is less than 1% of the laser flux power used, so it is expected to not have an impact. Nevertheless, a value of 5 Wm^{-2} K^{-1} was used as the convective coefficient and an ambient temperature of 293 K.

As initial conditions, the bulk density of *solid* is calculated as a fraction of the TMD (Eq. (9)). The initial density of the *gas*, $\rho_{g,0}$, is calculated by Eq. (5) based on an atmospheric pressure and initial temperature of 293 K.

3.3. Thermophysical and reaction parameters

The accurate estimation of the thermophysical and combustion properties of the system is needed for experimental validation. A baseline case was performed by setting all thermophysical and combustion properties ($C_{v,g}$, $C_{p,g}$, R, λ_{eff}, μ, d_c, A_0, and E_a) based on the sensible estimates from existing literature. In order to characterize the relative importance of these parameters on the physical phenomena driving the nanothermite combustion, a sensitivity analysis was performed on these variables. The values of the baseline case and parametric study are summarized in Table 1. For each thermophysical condition, the porosity of the pellet, ϕ, was varied from 0.1 to 0.9 (corresponding to 90–10% TMD respectively). Since experimental results don't use packing densities above 80% TMD [2] and tend to go as low as about 6% TMD [4] when packed lightly, this range of porosity values is appropriate.

The exact composition of the gas generated is not known, but some works [9,18] have suggested that oxygen is formed due to the decomposition of CuO. Aluminum and copper vapour is also possibly present due to the high adiabatic flame temperature [8]. To address this uncertainty, we model the properties of the *gas* either as oxygen, aluminum or copper vapour. The specific heats will be temperature dependent for oxygen, but constant at 2844 K for the others gaseous species since their states vary between solid, liquid and gas in the simulated temperature range and we are interested in their gas state values. The choice of gas species will fix the relation between $C_{v,g}$, $C_{p,g}$ and R due to their thermodynamic relationship. The thermal conductivity was also varied to reflect possible dominant heat conduction modes. We expect the thermal conductivity to be a function of the material properties and of the porosity characteristics of the pellet. Although, we could have accounted for the effect of porosity on the effective thermal conductivity by using a parallel conductance formula, similar to [20], we opted to keep the effective thermal conductivity constant with respect to porosity in our study. By doing so, we can decouple the influence of the thermal conductivity from the porosity and permeability of the pellet. For the baseline case, we assumed the theoretical thermal conductivity of aluminum and copper oxide at stoichiometric conditions ($\lambda_{eff} = 65$ W M^{-1} K^{-1}). For the parametric study, we considered the experimentally-measured conductivity of consolidated aluminum pellets proposed by Stacy et al. [21], which provides a lower bound on conductivity ($\lambda_{eff} = 1$ W M^{-1} K^{-1}). At the other extreme, we considered the thermal conductivity of pure aluminum ($\lambda_{eff} = 100$ W M^{-1} K^{-1}), as it is significantly higher than most metals. These large bounds cover the representative thermal conductivities that are likely to arise in reacting Al/CuO nanothermite pellets.

The viscosity was parametrically varied to span the range of viscosity from gases and liquid metals. The baseline case uses the gas values due to the consensus that gas is generated during the reaction and thus advecting through the pores under a pressure gradient. Nanothermite pellets are a mixture of nano-sized particles, however SEM images show that the agglomerates are closer to micron sized [22]. Without knowing the exact geometry of the pores, we estimate the characteristic pore size by considering a spherical pore contained in a cubic volume of length equal to the diameter. By considering the volume of the cube and surface area of the pore, the ratio is $1/\pi d_{pore} \approx 0.318 d_{pore}$, which gives the characteristic pore size a close relationship to the actual pore sizes. Therefore, assuming spherical pores, the characteristic pore size ranged from the order of nanometers to micrometers.

The pre-exponential factor taken from [9] was used in the baseline case, but smaller values were also selected to examine the effect of slower reaction time scales. In Kim [15], the activation energy values were taken from the reaction of nano- to micron-sized aluminum particles in air. Activation energies reported in Stamatis et al. [11] and Ermoline and Schoenitz [10] are significantly higher, however their kinetic models were more advanced than the present model. The values from Kim [15] were used to span different possible chemical kinetic time scales.

The enthalpy of combustion is documented for stoichiometric Al/CuO mixtures to be 4.07 kJ g^{-1} [6]. As the reaction progresses from ambient to 2844 K, the products of alumina and copper metal are formed that have melting points of 2327 K and 1358 K, respectively. Using the full enthalpy of combustion will overestimate the temperature since the melting of these products is not accounted for in the present model. Therefore, we subtract the enthalpies of fusion for alumina and copper (1.09 and 0.21 kJ g^{-1}, respectively) from the enthalpy of combustion to more accurately reflect the expected temperature of combustion.

3.4. Numerical framework

The numerical implementation of the governing and transport equations in a two-dimensional, axisymmetric domain was done in Python. The open-source solver is freely accessible[1]; the parent repository also contains all the input files, simulation results and raw data of all the cases in this paper.

In the present work, the focus is on Al/CuO nanothermite pellet but the numerical framework can be generalized to any gas-generating nanothermite material. The conservation of mass (2a), (2b), momentum (3), and energy (6) equations for the two-phases are solved using finite-volume method. At each control surface, a first-order scheme is used to calculate the convective and diffusive fluxes. The temperature gradients in the diffusive flux are calculated using second-order central difference whereas other properties are interpolated to first-order. Time integration of the governing equations uses a first-order, explicit scheme in which the stability is ensured by maintaining Fourier and CFL numbers below their stability bounds for the selected numerical schemes.

The numerical framework solves the governing equation set in a segregated manner. The temperature-dependent thermophysical

[1] https://github.com/jmreppsUWGrad/2D-Nanothermite .

properties and the Darcy velocity fields are re-computed at the start of each time-step and are assumed constant over the small, Δt of time-advancement step. Similarly, the source terms for the energy and mass equations are computed at the start of the time-step. Given the very small time steps imposed by the numerical stability of the problem, the error resulting from constant source over the small Δt was minimized and allowed us to avoid the use higher-order treatment for these stiff differential equations (such as Strang splitting). The effect of the selected time step on the reaction is assessed in the temporal convergence study in Section 4. Using the computed source terms and velocity field, the conservation of mass is then applied. As the momentum equation is simplified to a time independent Darcy flow, it is used directly in the computation of the mass conservation equation. The boundary conditions are then applied on the pressure field which sets the ambient pressure of the combustion. As the thermodynamic conditions are fully prescribed at the external bounds of the pellet, mass advection at the boundary nodes is necessary to enforce the pressure and density. This permits the advective mass loss through the porous boundaries of the nanothermite pellet and maintains a consistent numerical boundary condition in the problem. The energy equation is then solved by applying the diffusion and advection for both phases. The laser heating and natural convection with the ambient boundary conditions are applied last.

The burn rate is usually determined using high-speed camera images, but in this paper the reaction progress was used, as seen in Kim [15], to calculate the instantaneous burn rate:

$$V_{cw} = \frac{d}{dt}\int_0^H \eta dz \tag{17}$$

where H is the height of the pellet. After ignition, the instantaneous burn rate was calculated at every time step and then arithmetically averaged over all time to obtain the average burn rate, $\bar{V}_{cw}$. The transient burn rates are shown in Fig. 7 in the following section.

4. Assessment of the numerical solver

A limited number of standardized, benchmark cases are available in the open literature for the validation of the heat and mass transport with chemical reactions in porous media. It is worth mentioning that some work is being actively pursued in the wood pyrolysis community, but benchmarking cases that are relevant to consolidated nanothermite combustion are currently unavailable. The assessment of the numerical solver was done in a number of steps. First, we evaluated the temperature distribution in a steady state heat transfer case against an analytical solution. Second, we compared the unsteady heat transfer case, on an axisymmetric domain, against an established porous media solvers. For this work, we validated the results using Porous material Analysis Toolbox (PATO) which leverages the differential equation framework from OpenFOAM [23]. Finally, we conducted a spatial and temporal convergence study on the reacting nanothermite pellet case.

4.1. Validation: steady heat transfer

We first consider a square, planar domain in a steady state heat transfer. In this case, three side walls have a unitary temperature boundary condition, the top wall has a temperature value of T=2. The tractability of the steady-state partial differential equations means that an analytical solution that can be used to validate the heat transfer of the numerical solver. The analytical solution of this problem with the prescribed boundary conditions reads:

$$T = 1 + \frac{4}{\pi}\sum_{n=1}^{\infty}\left(\frac{\sin[(2n-1)\pi x]\sinh[(2n-1)\pi y]}{(2n-1)\sin[(2n-1)\pi]}\right) \tag{18}$$

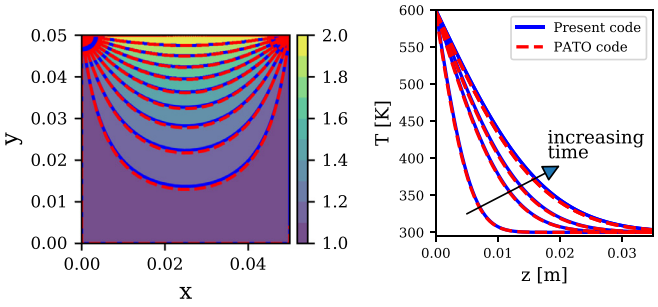

Fig. 2. Left: Steady-state heat transfer solution (blue lines and color) compared to analytical solution (dashed red line). Right: Evolution of the temperature along the centerline of the axisymmetric wedge with non-uniform heating at time 10, 40, 60 and 100 s. (For interpretation of the references to color in this figure legend, the reader is referred to the web version of this article.)

Figure 2 (left) shows the good agreement of the numerical solver and the analytical solution for this simple problem.

4.2. Validation: transient heat transfer

In the second case, we consider a two-dimensional, wedge (axisymmetric) with a height and radius of 0.05 m. The material properties are set as: density $\rho_s = 1000$ kg/m^3, specific heat $c_p =$ 1000 J/(kg·K), and thermal conductivity λ =1 W/(m·K). The 300 K initial temperature wedge is heated at the upper boundary about the central axis of the wedge to 600 K over a radius of 0.025 m; all the other side walls are set to a zero gradient boundary condition. Here we only assume heat transfer within the wedge without any underlying advective mass transport. This simple test case allows a direct assessment of the unsteady heat transfer characteristics of the code in an axisymmetric domain. The results of our numerical solver are compared to the solution of the identical case computed using Porous material Analysis Toolbox (PATO) [23]. Figure 2 (right) shows temperature evolution along the side wall of the wedge at various time instances.

4.3. Verification: spatial convergence

A mesh independence study was performed on a reactive, axisymmetric case. To assess spatial convergence, we consider the maximum local pressure during the entire combustion of the nanothermite pellet. For this case, we selected the permeability based on particle diameter of $d_c = 1\mu$m and porosity of $\phi = 0.3$. This test case was selected as it falls in a regime which is characterized by both conduction and convection; thus it represents a more challenging case to achieve grid convergence. Furthermore, the maximum pressure, over the entire pellet combustion, represents a highly-sensitive quantity that can be used to assess the adequacy of the mesh resolution. The maximum pressure as a function of the grid resolution is shown in Fig. 3 (left). For a grid resolution greater than about 100 000 nodes tend to converge to the same value within 1% which confirms that the selected mesh (around 300 000 nodes in our subsequent simulations) is appropriate for all the simulation results. Other metrics, such as reactive front propagation speed, Darcy velocity, temperature field were also assessed and converge more rapidly than maximum pressure.

4.4. Verification: temporal convergence

As we have a tightly-coupled set of equations which are solved in a segregated manner, the effect of the time step on the reaction is assessed. The stability of the numerical schemes dictates the upper limit of the time step but the highly non-linear source term with a segregated fluid solver may impose a more severe time-step

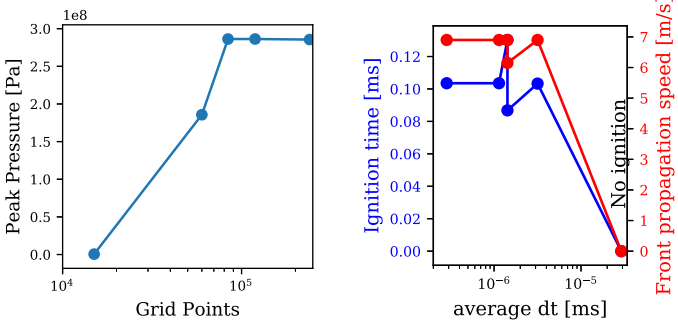

Fig. 3. Left: Mesh sensitivity study for maximum pressure within the domain. Right: Temporal convergence of the reactive simulations. The ignition time of the simulation and the average reactive front propagation speed at t=0.2 ms is evaluated.

restriction than the numerics alone. To evaluate the influence of the time advancement on the solution, we select the baseline configuration case (discussed in the previous section) with a porosity of 0.7 and modify only the time step of the simulation through the modification of the Fourier (Fo) and Courant-Friedrichs-Lewy (CFL) number. An adaptive time step is computed based on the minimal dt necessary to satisfy both the imposed Fo and CFL numbers over all the computational domain, therefore the systematic variation of either of the parameter is sufficient to assess the temporal convergence. Note that up until the time of ignition, the Fourier number dictates the time step of the simulation (as there is only thermal diffusion), as a result the time step is much larger than in the post-reaction time-step which is dictated by the convective constraint imposed by the CFL number. For comparative purposes, we present the results in terms of the average dt until $t = 0.2$ ms (ignition occurs at around $t = 0.1035$ ms). We evaluate the effect of the time step on both the ignition time and the average reaction front propagation speed (at $t = 0.2$ ms)–both these quantities would be directly affected by the highly non-linear source term. Figure 3 (right) shows the change of these critical quantities with the variation of the average time step until $t = 0.2$ ms. We note that if the time step is too large–although still below the numerical stability limit–ignition is impeded. We also note that varying the Fourier number alone (as was done at around 9×10^{-5} ms in Fig. 3 (right)) while maintaining the same average time, can greatly impact the ignition time but has a limited influence on the front propagation speed. All of the simulations in the present paper were conducted at a CFL< 0.1–which is far below the numerical stability–results in an average below $dt = \mathcal{O}(1 \times 10^{-6})$ ms. This gives us confidence in the selected time step for our simulations.

5. Results and discussion

5.1. Burning regimes

The results of the non-dimensionalization and the numerical study confirm previous experimental observations on the presence of convection- or conduction-dominated burning regimes. In loosely packed pellets (low TMD), burn rates increase significantly due to the strong advection through the higher porosity pellets [3,5]. This is first demonstrated with the Peclet number in Fig. 4 which shows an exponential decrease with increasing packing density. Here, the Peclet number is defined uniquely based on the characteristic scales of the problem (Eq. (15)) and not on numerical results. Note that many of the cases overlap with the baseline case in this figure. At higher packing densities, conduction is enhanced by the lower void fraction and the advection of the burnt gaseous products is impeded compared to the lower density pellets. The thermal state of the *gas* and kinetic parameters do not

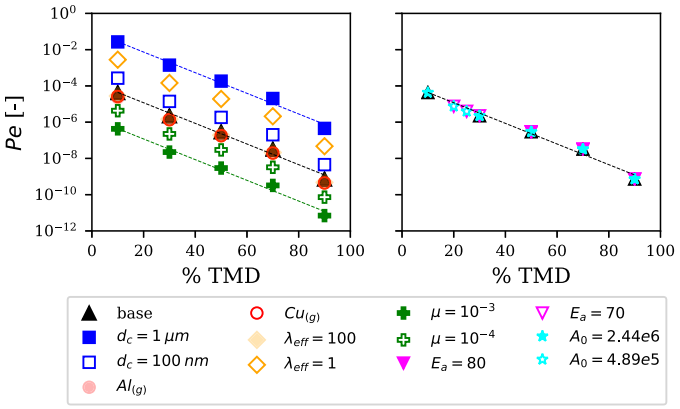

Fig. 4. Peclet number versus packing density for all simulation data. (a) corresponds to the variation of transport properties; (b) isolates the chemical kinetic parameters.

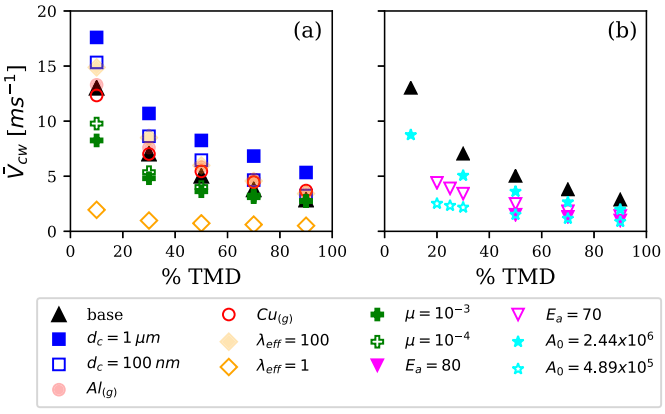

Fig. 5. Burn rate versus packing density for all simulation data. (a) corresponds to the variation of transport properties; (b) isolates the chemical kinetic parameters.

have an impact on the global Peclet number definition (based on our non-dimensionalization from the previous section). As the reaction timescale of the nanothermites is significantly smaller than either the advective or conductive transport timescale, a change in the reaction timescale does not impact the burning regime (see Fig. 4, right) as it does not enter our non-dimensionalization of the Peclet number.

The effect of the selection of the transport properties is apparent when plotting the burn rate (as measured from the numerical simulations) with respect to the packing density, as shown in Fig. 5. Thermal conductivity and viscosity have significant impacts on the burn rate of low density pellets whereas the characteristic pore size affects all ranges of TMD. Since advection is not significant at high densities, viscosity should not be as important, however the characteristic pore size still has an impact on the burn rate. Not too surprisingly, the reaction kinetics show a strong influence on the burn rate. It is also noticeable that the *gas* characteristics do not have a significant impact on the burning rate.

Given that the Darcy velocity characterizes the advection portion of the Peclet number and the velocity is strongly dependent on the permeability, there should be a significant impact of the packing density of the pellets on the burn rate. Analyzing the velocity contours for the baseline case at 90 and 10% TMD shown in Fig. 6, the velocity difference is evident.

The contours in Fig. 6 represent a snapshot of the Darcy velocity at a steady burn rate; these cases are shown at normalized times of 0.62 and 0.48 for 90% and 10% TMD, respectively. After ignition, the burn rate initially increases with time until a steady

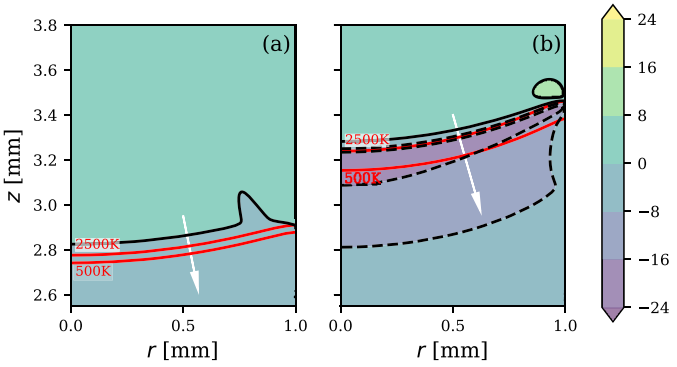

Fig. 6. Axial Darcy velocity (units ms^{-1}) contours for 90% (a) and 10% (b) TMD near the reaction front at the middle of the pellet. The isothermal lines at T=500K and 2500K are overlaid to illustrate the pre-heat zone in the pellet. The arrows indicate the approximate direction of the propagating reactive front.

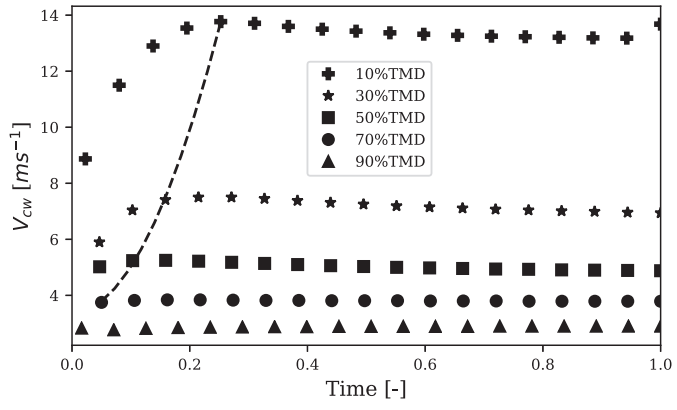

Fig. 7. Transient burn rate data for baseline cases. The dashed line corresponds to the approximate delineation between the conduction- (left of the line) and advection-dominating regimes.

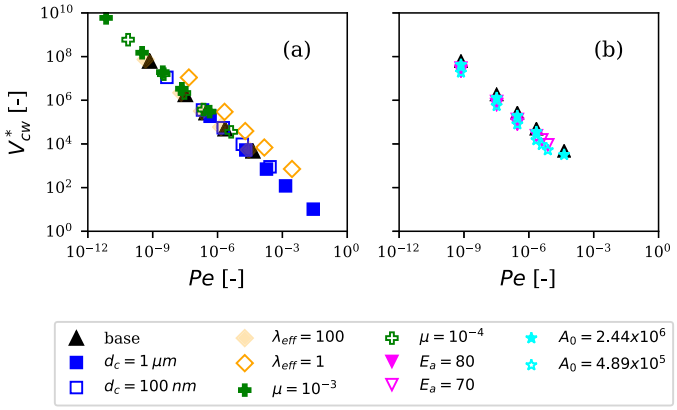

Fig. 8. Non-dimensional burn rate versus Peclet number for simulation data. (a) corresponds to the variation of transport properties; (b) isolates the chemical kinetic parameters.

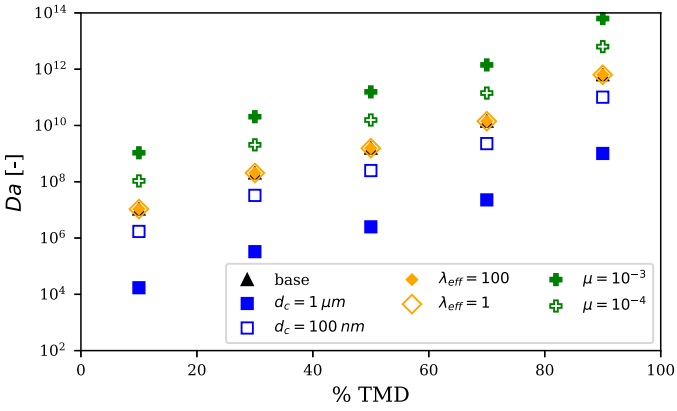

Fig. 9. Damköhler number versus packing density for transport parameters.

burn rate is reached. With an increase in the Darcy velocity at low packing densities, we observe an increasingly large pre-heat zone as observed by the isothermal lines at 500 and 2500K in this same figure. As a Dirichlet boundary condition is imposed on the outer walls of the pellet, a pressure gradient can develop which causes the formation of small pockets of positive velocity Darcy flow, see Fig. 6(b) at (r, z) =(0.95,3.45).

Figure 7 shows the transient burn rate data for the baseline runs. Since the ignition time, burn rate, and extinction time vary among all cases, the average burn rate is plotted as a function of the normalized time. We recall that the simulations are run until 80% of the pellet is consumed which is used to map the burn time between 0 and 1. An interesting observation is that at lower packing densities, it takes longer to achieve a steady burn rate. Before self-sustained ignition, the main thermal propagation mechanism is driven by conduction since minimal *gas* is generated, thus pressure, necessary to drive the Darcy flow, does not have sufficient time to build in the pellet. This regime is characterized by a nearly linear increase in the burn rate. The duration of this conduction-dominated regime is highly dependent on the packing density of the pellets—the higher the packing density, the shorter the conductive-dominated regime. Once the ignition is self-sustained, *gas* is generated at a faster rate and contributes to an enhanced burning rate through a pressure-driven, advection-dominated flow; this is most specifically observed at the lower densities. The dashed curve plotted in Fig. 7 shows the approximate transition from conduction- to advection-dominated burning regimes. For densities of 50% TMD and higher, the steady burn rate is achieved faster since the permeability inhibits advection and thermal diffusivity is enhanced with lower porosity. Thus for high packing density, conduction always dominates.

The effect of conduction and advection can also be inferred from non-dimensionalizing the average burn rate ($V^*_{cw} = \bar{V}_{cw}/U_{ref}$) and plotting it with respect to the Peclet number. As shown in Fig. 8, a predictable trend of burn rate as a function of the Peclet number is apparent. The major contributors to this trend are the flow- and conduction-determining parameters; the chemical kinetic parameters collapse on the baseline results. While there is a clear relationship with the Peclet number and non-dimensional burn rate, there is a significant deviation between the lowest and highest thermal conductivity cases. Although the definition of Peclet number is based on the thermal conductivity, the Peclet number alone cannot be used to characterize the transport phenomena occurring. In this paper each parameter is treated independently, however in reality the thermal conductivity and characteristic pore size would be related through the nature of the pore structure, more will be discussed in Section 5.4. The thermal state of the *gas* followed the trend in Fig. 8 but was removed due to overlapping data points. The chemical kinetic parameters show little influence on the normalized burn rate.

The Damköhler number defines the ratio of advection to the reaction time scale. Based on the present non-dimensionalization of the Damköhler number (Eq. (16)), increasing density has a two-fold effect. Advection is decreased due to a lower porosity with increasing TMD. This contributes to the linear trend (in a semi-log plot) observed in Fig. 9. Based on the non-dimensionalization, the characteristic size of the nanothermites can significantly affect the

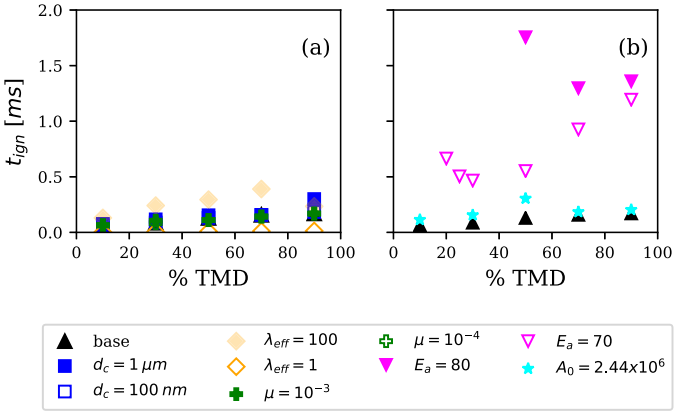

Fig. 10. Ignition delay versus packing density for simulation data. Variation of the transport (a) and chemical kinetic (b) parameters.

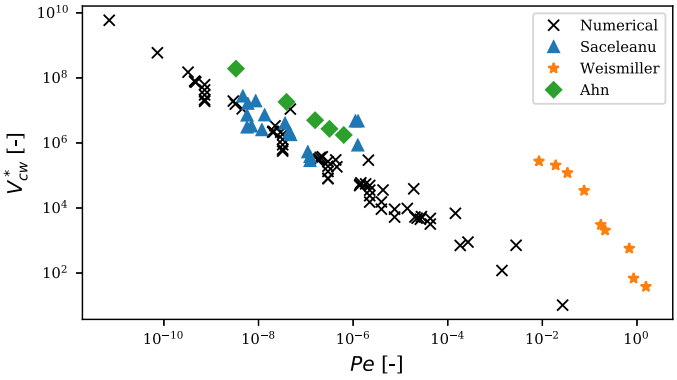

Fig. 11. Comparison of the present non-dimensional numerical results with published experimental results by Saceleanu et al. [3], Weismiller et al. [4], and Ahn et al. [2].

Damköhler number given that the permeability, and concomitantly, the characteristic Darcy velocity is proportional to the square of the characteristic dimension in the Kozeny-Carmen equation, see Equation (4).

5.2. Ignition delay

Of the literature examined, only Saceleanu et al. [3] reported the ignition delay which they defined as the time before the reaction front was formed. This observation was confirmed by high-speed images and photodiode detection of intermediate species. The numerical results presented in Fig. 10 support their findings as far as the linear behaviour with respect to packing density, but the numerical results are about one order of magnitude smaller. Numerically, the ignition delay was determined based on the heat released from the reaction surpassing, by one order of magnitude, the conductive and convective losses. Once this condition was met on a finite number of cells within the computational domain (in our simulations, we selected 10 cells as the threshold), we determined the pellet to be ignited. The heuristics used herein may explain the much shorter ignition time compared to experiments.

The thermal conductivity is the only transport property in Fig. 10 that has a significant impact on the ignition delay. This supports the observation of a conduction-dominated initial regime in the transient burn-rate in Fig. 7. Higher density results in more heat released, but also more capacity for heat storage. Considering an energy balance near the pellet surface, the laser heats the pellet which then diffuses, advects with the *gas* or gets stored within the internal energy of the system. Higher heat storage requires more heat input to raise the temperature of the pellet to ignition. Since the reaction has not started, *gas* has not been generated, thus advection is not significant. Therefore, thermal conductivity should be the dominating factor in ignition delay. Data points are missing for both activation energy studies because ignition in the model was not achieved for those packing densities. Even from this data, an exponential trend is developing as the packing density reduces. For all other parameter changes, the ignition delay is consistently higher at densely packed pellets, however a local minimum in ignition delay appears at higher activation energies and low pre-exponential values. From the previous Figs. 4, 5 and 8, only ignition delay is significantly affected by these parameters. More will be discussed in Section 5.4.

5.3. Non-dimensionalization and experimental comparison

Using the experimental data from Saceleanu et al. [3], Weismiller et al. [4], and Ahn et al. [2], the non-dimensionalization techniques presented in this work can be used to compare the present numerical with published experimental results. In order to compare our numerical simulations with published experimental data, a number of assumptions must be made to supplement the available information from the respective papers. The characteristic pore size was calculated with the reported specific surface area of the particles used to synthesize the compounds and the TMD of Al/CuO nanothermites to obtain an equivalent length scale representing the surface area and volume ratio. Brunauer-Emmett-Teller (BET) specific area of the as-received particles was used to quantify the powders used to synthesize the thermites in Ahn et al. [2] and Saceleanu et al. [3]. This characterizes the surface area of the particles normalized by the mass. Using this in conjunction with the bulk density, the solid volume to fluid-solid interfacial surface area ratio can be used to estimate d_c. The BET specific areas for the as-received particles reported in Saceleanu et al. [3] and Ahn et al. [2] range between 5 and 50 $m^2\,g^{-1}$ which would correspond to values of between 9.7×10^{-9} and 3.91×10^{-8} m for d_c. Given how close Saceleanu and Ahn's data were to our numerical results, the BET specific areas can provide a reasonable estimate of the characteristic pore size. Due to the lack of information on the powder size in the Weismiller et al. [4] experiments, we selected $d_c = 3.8 \times 10^{-8}$ m. Naturally, d_c greatly impacts the permeability estimation which in turn influences the characteristic velocity which is used in both the Pe and V^*_{CW} terms. The effective thermal conductivity was calculated as a mass fraction mixture of aluminum and copper oxide at the reported equivalence ratios, here we did not account for the change in porosity on the thermal conductivity. For Saceleanu et al. [3] thermal conductivity varied between 71 and 97 $Wm^{-1}\,K^{-1}$, the value fixed at 97 and 74 $Wm^{-1}\,K^{-1}$ respectively for Ahn et al. [2] and Weismiller et al. [4]. The experiments by Weismiller et al. were conducted at different ambient pressures, so the reference pressure was changed accordingly in the non-dimensionalization.

From Fig. 11, the experimental results from Saceleanu et al. show very close agreement to the numerical results in the present study. Ahn's data are in line with the lowest thermal conductivity case seen in Fig. 8. From the observations in Section 5.1, decreasing the characteristic pore size and setting a lower value of conductivity ($\lambda_{eff} = 1$ $Wm^{-1}\,K^{-1}$) would shift the numerical results in Fig. 11 which would result in a closer to Ahn et al.'s data. This suggests that the thermal conductivity values proposed by Stacy et al. [21] would result in a closer match to Ahn et al.'s experimental data.

The results by Weismiller et al. sit at the higher end of Peclet number range suggesting the pellets were more porous, hence more convective heat transfer is present. The departure of the

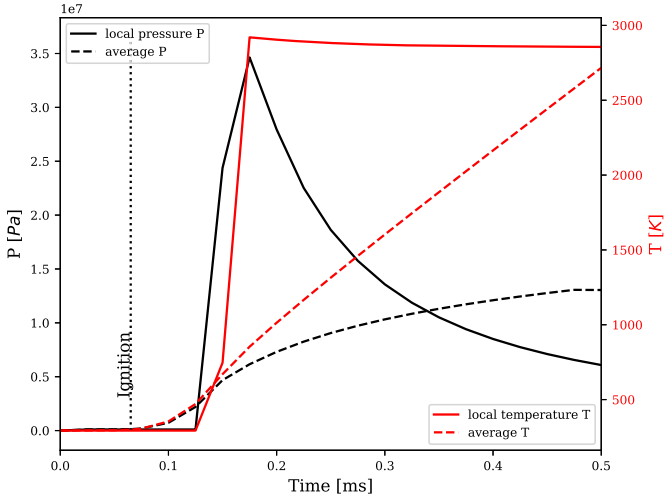

Fig. 12. Pressure and temperature evolution at 1 mm from the top and 0.5 mm from the centre of the pellet for 10% TMD. The average pressure and temperature in the entire pellet is overlaid (dashed lines).

Weismiller et al. results with the other experiments is significant. The exact reason for this is unclear but could be related to the incorrect estimation of d_c (Weismiller et al. does not provide the BET specific areas for the as-received particles) which inherently affects the estimation of permeability required for the non-dimensionalization. Additionally, the causes for the large error can be related to the non-dimensionalization itself (especially since we non-dimensionalize with respect to ambient pressure instead of pressure gradient in the definition of the characteristic velocity), incorrect estimation of the material properties or some of the other estimations noted above.

Despite the overall good collapse of the experimental and numerical data, we do acknowledge the strong dependence on the reference velocity, U_{ref}, for the variables on the abscissa and ordinate axes. As the characteristic velocity is used to non-dimensionalize the mean reaction front velocity (denominator) and in the numerator in the definition of the Peclet number (Eq. (15)), this enhances the coupling among the variables along the axes.

Researchers report burn rates for lower densities pellets around 100 or 1000 ms^{-1} which is significantly higher than the values reported in this paper (maximum 18 ms^{-1}) which means there are additional factors not properly reflected in this model. The current model considers advection of gases which have significantly lower density than their liquid counterparts. Convection of condensed phases was specified as a likely mechanism for producing the large burn rates [5] with evidence present in some experiments [24] and suggested as plausible in others [1,4,25]. Liquids have larger viscosity values than gases, which Fig. 4 suggests conduction would be the dominating propagation mechanism and Fig. 5 show a reduction in burn rate. When comparing the advection term in Eq. (6) with viscosity in Eq. (3), this change in density and viscosity between the liquid and gaseous state may play an important role. The existing model is able to capture the effect of advective heat transfer at lower densities, but falls short, by an order of magnitude, to estimate the burn rates.

Pressure has been measured and predicted for Al/CuO nanothermite combustion in previous literature. Sanders et al. [1] measured pressures around 1 MPa for loose powders (about 6% TMD) in a pressure cell and 10 MPa in low density burn tube experiments. Weismiller et al. [4] measured 10 MPa at 6.6% TMD and Baijot et al. [8] proposed a theoretical model for the pressure evolution of Al/CuO thermite reaction which varies between about 10 and 110 MPa. The results of this study show peak pressure values between 10 MPa at low densities and 90 GPa at higher densities which is higher than most experiments and numerical estimate. It should be noted that these pressure values correspond to the local maximum pressure within the pellet and not an integrated pressure value which would be computed from experimental measurements. The average pressure within the computational domain remains more in line with the experimental results, the average pressure varies from 13 MPa to 1.4 GPa at the times of peak pressure for the baselines cases. At high densities, more gas is generated and the low porosity results in higher pressures (by Eq. (5)) however, the pellet is likely to disintegrate at these pressures nullifying the assumptions of this model. The average transient pressure data for the baseline at 10% TMD is shown in Fig. 12 which is in good qualitative agreement with the transient pressure data reported in Sanders et al. [1] and Baijot et al. [8]. Therefore, pressure can be predicted with some accuracy for lower densities, but becomes unphysically high at higher densities.

The temperature evolution is also plotted in Fig. 12 which approaches the adiabatic flame temperature. According to calculations done in Sanders et al. [1], the adiabatic flame temperature varies with equivalence ratio and Weismiller et al. [4] showed it varies with ambient pressure. The reaction model is too simple to consider these factors, so Fig. 12 serves as a confirmation that temperatures are not significantly different than the adiabatic flame temperature for stoichiometric reactions from Fischer and Grubelich [6].

5.4. Discussion

Based on the results in Figs. 4, 5, 8, 9 and 10, the thermal conductivity has a strong dependence on the reaction characteristics, particularly with regards to ignition. Conduction is generally accepted as the dominant reaction-propagation mechanism for dense pellets, especially in the early stages of combustion, whereas convection tends to dominate in less dense setups. When non-dimensionalizing the experimental data in Fig. 11, thermal conductivity is estimated using the equivalence ratios reported and assuming no porosity. Correlating porosity and effective conductive properties in porous media has been the subject of some studies [19,20,26] that summarize existing theoretical models. Theoretical models to predict effective conductivity are derived based on assumptions about the size and distribution of the pores [20]. In general, they can only be used for simple structures and cannot be used to predict the properties of new materials [19]. Due to the significant difference in thermal conductivities of gases and solids, the upper and lower bounds of possible effective property values for porous media is significant. Without being able to quantify the pore structure, an appropriate thermal conductivity model or value is prone to a high level of uncertainty.

Quantifying the pore structure also helps to identify the value of the characteristic pore size. This is the dominant variable in Eq. (4) to determine the permeability through the porous pellet (thus, reference velocity also). Quantifying the pore structure has not been done in consolidated nanothermite pellets and, based on Figs. 4, 5, and 9, there is a strong sensitivity which makes this parameter even more important. Since the reference velocity is present in the Peclet and non-dimensional burn rate, both groups are equally affected whereas the thermal conductivity effect is mainly on the Peclet number.

The chemical kinetic parameters only moderatly affect many trends observed herein except the ignition delay in Fig. 10. The way in which ignition delay is defined varies in the literature, however, in this numerical implementation, it is defined as when the heat released is an order of magnitude higher than the conduction and advection heat losses in at least 10 computational cells. For

this reason, the values of ignition delay are not directly comparable to literature, but the trends can be. The trend is mostly linear with density, however with increasing activation energy, an exponential form emerges.

The activation energy and pre-exponential factor were chosen as an estimate for the reaction mechanism and time scales since various values are used in literature. The reaction is estimated with a simple model and since the chosen values were taken from different sources, there might also be a non-physical pairing of values which taint the results. Another important aspect also governing ignition delay is ablation due to laser heating. This was observed in Al/CuO experiments of Saceleanu et al. [3] and studied in Stacy et al. [14] for Al/MoO3 nanothermite pellets which found that ignition delay increases when more material is ablated during preheating. The presented model does not account for ablation.

6. Conclusion

A continuum model of Al/CuO nanothermite pellet combustion was presented which utilized a two-phase model coupled with Darcy's law, and the transient heat equation. This finite volume numerical framework solves the governing equations on a two-dimensional, axisymmetric domain; the code is freely available for further development. The primary objective was to model the porous media flow resulting from the porosity of the compressed nanothermite pellet, thus a simplified reaction model was used to approximate the reaction kinetics. A non-dimensional analysis based on the governing equations and characteristic Darcy velocity was used to evaluate the burning regimes of nanothermite pellet combustion. The results support the experimental observations of conduction and convection burning regimes based on packing density, however the model is not able quantitatively capture the experimentally observed burn rates at low packing density. Despite this, non-dimensionalization of the numerical results with published experimental studies show good agreement.

Ignition delay trends are similar to the literature, however the ignition time is lower by an order of magnitude. This can be related to the metric used to determine ignition in the numerical simulations. Ablation of surface particles is another possible reason for this discrepancy due to the heat that is applied by the laser but not used to heat up the pellet to ignition. The model is most sensitive to the nature of the pore structure. Better quatification of the porous structure will reduce the uncertainty in choosing appropriate values for thermal conductivity and characteristic pore size. Literature has suggested convection of condensed phases as sources of higher burn rates, so future development of this model should try and incorporate this multi-phase situation with the porous medi a considerations presented here.

Declaration of Competing Interest

The authors declare that they have no known competing financial interests or personal relationships that could have appeared to influence the work reported in this paper.

Acknowledgments

Financial support from the Natural Sciences and Engineering Research Council (NSERC) is acknowledged. The computational resources were provided through support from SciNet and Compute Canada. JME would like to recognize the support from Ontario Graduate Scholarship (OGS) and the University of Waterloo Graduate Student Fellowship.

References

[1] V.E. Sanders, B.W. Asay, T.J. Foley, B.C. Tappan, A.N. Pacheco, S.F. Son, Reaction propagation of four nanoscale energetic composites (Al/MoO3, Al/WO3, Al/CuO, and B12O3), J. Propul. Power 23 (4) (2007) 707–714, doi:10.2514/1.26089.
[2] J.Y. Ahn, J.H. Kim, J.M. Kim, D.W. Lee, J.K. Park, D. Lee, S.H. Kim, Combustion characteristics of high-energy Al/CuO composite powders: the role of oxidizer structure and pellet density, Powder Technol. 241 (2013) 67–73, doi:10.1016/j.powtec.2013.03.017.
[3] F. Saceleanu, M. Idir, N. Chaumeix, J.Z. Wen, Combustion characteristics of physically mixed 40 nm aluminum/copper oxide nanothermites using laser ignition, Front. Chem. 6 (2018) 1–10, doi:10.3389/fchem.2018.00465.
[4] M.R. Weismiller, J.Y. Malchi, R.A. Yetter, T.J. Foley, Dependence of flame propagation on pressure and pressurizing gas for an Al/CuO nanoscale thermite, Proceedings of the Combustion Institute, 32, The Combustion Institute (2009), pp. 1895–1903, doi:10.1016/j.proci.2008.06.191.
[5] G.C. Egan, M.R. Zachariah, Commentary on the heat transfer mechanisms controlling propagation in nanothermites, Combust. Flame 162 (7) (2015) 2959–2961, doi:10.1016/j.combustflame.2015.04.013.
[6] S. Fischer, M. Grubelich, A survey of combustible metals thermites and intermetallics for pyrotechnic applications, 32nd AIAA Joint Propulsion Conference (1996), p. 15, doi:10.2514/6.1996-3018.
[7] S.W. Dean, M.L. Pantoya, A.E. Gash, S.C. Stacy, L.J. Hope-Weeks, Enhanced convective heat transfer in nongas generating nanoparticle thermites, J. Heat Transf. 132 (11) (2010) 111201, doi:10.1115/1.4001933.
[8] V. Baijot, L. Glavier, J.-M. Ducéré, M. Djafari-Rouhani, C. Rossi, A. Estève, Modeling the pressure generation in aluminum based thermites, Propellants Explos. Pyrotech. 40 (3) (2015) 402–412, doi:10.1002/prep.201.
[9] S.M. Umbrajkar, M. Schoenitz, E.L. Dreizin, Exothermic reactions in Al-CuO nanocomposites, Thermochim. Acta 451 (1–2) (2006) 34–43, doi:10.1016/j.tca.2006.09.002.
[10] A. Ermoline, M. Schoenitz, E.L. Dreizin, Reactions leading to ignition in fully dense nanocomposite Al-oxide systems, Combust. Flame 158 (6) (2011) 1076–1083, doi:10.1016/j.combustflame.2010.10.010.
[11] D. Stamatis, A. Ermoline, E.L. Dreizin, A multi-step reaction model for ignition of fully-dense Al-CuO nanocomposite powders, Combust. Theor. Model. 16 (6) (2012) 1011–1028, doi:10.1080/13647830.2012.694480.
[12] V. Baijot, D.R. Mehdi, C. Rossi, A. Estève, A multi-phase micro-kinetic model for simulating aluminum based thermite reactions, Combust. Flame 180 (2017) 10–19, doi:10.1016/j.combustflame.2017.02.031.
[13] A. Nicollet, G. Lahiner, A. Belisario, S. Souleille, M. Djafari-Rouhani, A. Estève, C. Rossi, Investigation of Al/CuO multilayered thermite ignition, J. Appl. Phys. 121 (3) (2017), doi:10.1063/1.4974288.
[14] S.C. Stacy, R.A. Massad, M.L. Pantoya, Pre-ignition laser ablation of nanocomposite energetic materials, J Appl Phys 113 (21) (2013), doi:10.1063/1.4808458.
[15] K. Kim, Computational Modeling of Combustion Wave in Nanoscale Thermite Reaction, International Journal of Energy andPower Engineering 8 (7) (2014) 612–615. 10.1999
[16] S. Knapp, N. Eisenreich, S. Kelzenberg, E. Roth, V. Weiser, Modelling of Al/MnO2 and Ti/MnO2 thermite mixtures, Propellants Explos. Pyrotech. 44 (6) (2019) 706–713, doi:10.1002/prep.201800347.
[17] M.M. Kaviany, Principles of Heat Transfer in Porous Media, Mechanical engineering series, second ed., Springer-Verlag, New York, 1995.
[18] G. Jian, S. Chowdhury, K. Sullivan, M.R. Zachariah, Nanothermite reactions: is gas phase oxygen generation from the oxygen carrier an essential prerequisite to ignition? Combust. Flame 160 (2) (2013) 432–437, doi:10.1016/j.combustflame.2012.09.009.
[19] M. Wang, N. Pan, Predictions of effective physical properties of complex multiphase materials, Mater. Sci. Eng. R 63 (1) (2008) 1–30, doi:10.1016/j.mser.2008.07.001.
[20] K. Pietrak, T. Wiśniewski, A review of models for effective thermal conductivity of composite materials, J. Power Technol. 95 (1) (2015) 14–24.
[21] S.C. Stacy, X. Zhang, M. Pantoya, B. Weeks, The effects of density on thermal conductivity and absorption coefficient for consolidated aluminum nanoparticles, Int. J. Heat Mass Transf. 73 (2014) 595–599, doi:10.1016/j.ijheatmasstransfer.2014.02.050.
[22] I. Monk, M. Schoenitz, R.J. Jacob, E.L. Dreizin, M.R. Zachariah, Combustion characteristics of stoichiometric Al-CuO nanocomposite thermites prepared by different methods, Combust. Sci. Technol. 189 (3) (2017) 555–574, doi:10.1080/00102202.2016.1225731.
[23] J. Lachaud, J. Scoggins, T. Magin, M. Meyer, N. Mansour, A generic local thermal equilibrium model for porous reactive materials submitted to high temperatures, Int. J. Heat Mass Transf. 108 (2017) 1406–1417, doi:10.1016/j.ijheatmasstransfer.2016.11.067.
[24] V.I. Levitas, M.L. Pantoya, S. Dean, Melt dispersion mechanism for fast reaction of aluminum nano- and micron-scale particles: flame propagation and SEM studies, Combust. Flame 161 (6) (2014) 1668–1677, doi:10.1016/j.combustflame.2013.11.021.
[25] J.J. Granier, M.L. Pantoya, Laser ignition of nanocomposite thermites, Combust. Flame 138 (4) (2004) 373–383, doi:10.1016/j.combustflame.2004.05.006.
[26] R. Askari, S. Taheri, S.H. Hejazi, Thermal conductivity of granular porous media: apore scale modeling approach, AIP Adv. 5 (9) (2015), doi:10.1063/1.4930258.